Thin Solid Films 693 (2020) 137680

Contents lists available at ScienceDirect

Thin Solid Films

journal homepage: www.elsevier.com/locate/tsf

Microstructure and thermal conductivity of Ti-Al-Si-N nanocomposite coatings deposited by modulated pulsed power magnetron sputtering

H. Chen, B.C. Zheng, Y.X. Ou, M.K. Lei*

Surface Engineering Laboratory, School of Materials Science and Engineering, Dalian University of Technology, Dalian 116024, China

ARTICLE INFO

Keywords:
Thermal conductivity
Grain size
Titanium aluminum silicon nitride
Transient thermoreflectance technique

ABSTRACT

Hard Ti-Al-Si-N coatings are widely used in cutting tools, due to their excellent mechanical properties and superior thermal properties. In this study, Ti-Al-Si-N coatings are deposited by modulated pulsed power magnetron sputtering, with various substrate bias voltages from −35 V to −130 V. As the bias voltage goes up, the composition of coatings remained nearly unchanged, maintained as a constant of $Ti_{0.18}Al_{0.26}Si_{0.05}N_{0.51}$. However, the Ti-Al-Si-N coatings have a decrease in (200)-preferred orientation; dense columnar structure (Zone I) of Ti-Al-Si-N coatings gradually evolves into featureless and flat cross sections structure (Zone T). As increasing the substrate bias voltage, the hardness increases from 31.2 GPa to 37.5 GPa, the H/E* value increases from 0.079 to 0.090, while the compressive residual stress of coatings raises from -1.22 GPa to -2.15 GPa. The thermal conductivity of coatings is examined by transient thermoreflectance technique, which decreases from 5.4 W/m*K to 2.1 W/m*K with the bias voltage. The values of electric resistivity ρ for all coatings are very large, ranging from 147 kΩ·m to 173 kΩ·m. The electronic thermal conductivity has no contribution to the thermal conductivity of Ti-Al-Si-N coatings, which is mainly determined by the phonon thermal conductivity. As increasing the substrate bias voltage, the average grain size of Ti-Al-Si-N nanocomposite coatings decreases from 16 nm to 5 nm. The interfacial density per unit volume is therefore increased, and leading to more interface scattering of the phonons in the heat transport progress, which is the key parameter in determining thermal conductivity of Ti-Al-Si-N nanocomposite coatings.

1. Introduction

In the past few decades, TiN hard coatings with high hardness and wear resistance have been widely used in the cutting tool industry for increasing the service lifetime. However, low oxidation resistance and poor thermal stability of TiN coatings limited their further development. Under high-speed cutting, TiN coatings couldn't meet a wide range of performance requirements, such as the high hardness, the toughness, as well as the wear, thermal and oxidation resistances, therefore they had been gradually replaced by TiAlN coatings [1–4]. The TiAlN coating is superior to TiN coating in terms of hardness, wear resistance, and especially oxidation resistance. The cutting temperature in the modern high-speed cutting industry can reach 1000 °C, which can cause oxidation and hardness decrease of the TiAlN coatings. In view of this, Ti-Al-Si-N nanocomposite coatings are now increasingly used on the cutting tools. Compared with traditional hard coatings of TiN, AlN or TiAlN, the Ti-Al-Si-N nanocomposite coating that forms a structure of amorphous Si_3N_4 wrap nanocrystalline TiAlN has attracted worldwide attention due to its superior properties [5–7]. By modulating the distribution and content of nanocrystalline TiAlN and amorphous phase Si_3N_4, the Ti-Al-Si-N coatings can obtain various excellent properties. Veprek et al. found that the Ti-Al-Si-N nanocomposite coating maintained a high hardness at the annealing temperature as high as 1000 °C [8]. Chang et al. [9] reported that the Ti-Al-Si-N coatings had an enhanced oxidation resistance up to 1115 °C, when the (Al + Si)/(Al + Ti + Si) composition ratio was about 0.66. According to the previous studies, the cutting performance of the Ti-Al-Si-N coated cermet tools had been significantly improved compared with that of the TiN and TiAlN coated cutting tools, especially in the condition of high speed cutting, which was above 200 m/min [10,11].

As discussed above, the Ti-Al-Si-N coatings are often exposed to high temperatures in the cutting process. To avoid oxidation and the hardness reduction of the coatings, the thermal properties, especially the thermal conductivity plays an important role. Thermal conductivity is an intrinsic property of the coating associated with the ability to conduct heat. For high speed cutting conditions, low thermal conductivity is beneficial, for it provides a thermal barrier layer and can effectively delay the temperature rise on the tool substrate materials.

* Corresponding author at: Surface Engineering Laboratory, School of Materials Science and Engineering, Dalian University of Technology, Dalian 116024, China
E-mail address: surfeng@dlut.edu.cn (M.K. Lei).

https://doi.org/10.1016/j.tsf.2019.137680
Received 29 April 2019; Received in revised form 18 October 2019; Accepted 29 October 2019
Available online 01 November 2019
0040-6090/

Bouzakis et al. [12] reported the temperature distribution of TiN, TiAlN and Ti-Si-N coated tools with the cutting speed of 200 m/min. The Ti-Si-N coated tools with the lowest thermal conductivity of 6.7 W/m*K had the lowest cutting temperature of 150 ℃. Fox-Rabinovich et al. [13] demonstrated that the multilayered TiAlN/Cu coatings had better cutting performance than TiAlN coatings, both coatings had similar mechanical properties, but thermal conductivity of TiAlN/Cu coatings was obvious lower than that of TiAlN coatings, which was the main reason for the improved cutting performance of the TiAlN/Cu coatings. Samani et al. [14,15] reported that the thermal conductivity of Ti-Al-Si-N coatings decreased from 4.1 W/m*K to 2.1 W/m*K with (Al + Si)/Ti contents ratio increased from 0.40 to 1.59, and the multilayer-Ti-Al-Si-N coatings decreased from 4.92 W/m*K to 3.20 W/m*K with the bilayer number increased from 5 to 100.

Ti-Al-Si-N coatings were prepared using Modulated Pulsed Power Magnetron Sputtering (MPPMS), which had significant advantages compared with conventional magnetron sputtering techniques, such as high plasma density and ionization rate [16]. By applying the substrate bias, the deposition energy and angle of ion species can be adjusted to modulate the microstructures and mechanical properties of the deposited coatings, e.g., the grain size, the orientation and the hardness, etc. In our previous work [17,18], we discussed the mechanical properties, the toughness and wear performance of Ti-Al-Si-N nanocomposite coatings under various peak powers and different Ar/N_2 gas ratios. However, thermal property of Ti-Al-Si-N coatings prepared by MPPMS has not been studied.

In this research, Ti-Al-Si-N coatings were prepared by MPPMS on the Si(100) substrate at different bias voltages. The thermal conductivity of coatings was measured by transient thermoreflectance technique and the mechanism of thermal conductivity was studied in the light of grain size through adjusting the bias voltage.

2. Experimental procedures

The Ti-Al-Si-N coating was prepared from a hot pressed $Ti_{0.47}Al_{0.47}Si_{0.06}$ (99.9% purity) target by MPPMS system [18]. The size of target was 44 cm × 14 cm × 0.6 cm, and the effective sputtering area of the target was 180 cm^2, which was used to calculate the peak power density of the target discharge. The target was powered by a Zpulser LLC MPP power source. Before deposition, a base pressure less than 2×10^{-4} Pa was achieved, and working pressure was maintained at 0.5 Pa. The working pressure was argon and nitrogen with a purity of 99.9%. The total gas flow rate was 80 sccm, and the $N_2/(N_2+Ar)$ ratio was 20%. The substrates were Si(100) wafers without additional heating, which were ultrasonically cleaned in acetone and alcohol for 20 min, respectively. The substrate holder surface was parallel to the target surface, the mean substrate-target distance was kept constant at 100 mm. The deposition temperature was measured by THERMAX surface temperature strips, these strips contained segments would turn black when a designated temperature was achieved. The strips can record the ranging temperature of 200–260 ℃ with an increment of 5 ℃, and the temperature raised from 215 ℃ to 245 ℃ with increasing bias voltage from −35 V to −130 V. Before the MPPMS deposition process, the substrate surface was bombarded for 20 min by using $a-350$ V pulsed DC bias at the working pressure of 2.5 Pa, the target was pre-sputtered for 2 min under a pressure of 0.5 Pa.

The length of MPPMS pulse waveform was 1000 μs, which consisted a weak ionization stage of 600 μs and a strong ionization stage of 400 μs, respectively [18]. The duty cycle term τ_{on}/τ_{off} of weak and strong ionization stage were 34/6 and 6/10, respectively. The Ti-Al-Si-N coatings were deposited for 120 min at the bias voltage from −35 V to −130 V. The detailed MPPMS pulsing parameters were displayed in Table 1.

The element composition of the Ti-Al-Si-N coatings was detected by electron probe microanalysis (EPMA, SHIMADZU EPMA-1600), the electron acceleration voltage was 15 kV and the backscatter electronic beam size was ϕ100 μm. The crystal structure was measured by X-ray diffractometer (XRD, PANalytical EMPYREAN) with a monochromatic CuKα radiation of 40 kV and 30 mA. The geometry was Bragg–Brentano with two-theta step of 0.02° and the time per a two-theta angle was 5 s. The crystallite size analysis was characterized by full width at half maximum (FWHM) values of fitted peak profiles at corresponding angles using a MDI Jade 5.0 software program. The cross-sectional microstructure of the coatings was characterized by a field emission scanning electron microscope (FESEM, ZEISS SUPRA ZEISS SUPRA-55 VP) with an operating voltage of 15 kV. The planar-view microstructure of the TiAlSiN coatings was examined by a high resolution transmission electron microscope (HRTEM, Tecnai 220S-TWIM) with an acceleration voltage of 200 kV. The samples for planar-view HRTEM observation were mechanically ground to 30 μm thick foil. And then, it was further reduced up to electron transparency using a Gatan Model 691 precision ion polishing with Ar^+ beam at 4 keV and 3–7° angle of beam-to-sample surface. The hardness and effective Young's modulus of coatings were examined by XP™ nanoindenter with a Berkovich diamond tip. For preventing the influence of the substrate, the indentation depth was less than 10% of the film thickness. The Stoney formula was used to calculate the macrostress of coating stress, by measuring the curvature change of the Si plate with a size of 30 × 5 mm before and after deposition [19].

Table 1
Deposition parameters of TiAlSiN coatings by MPPMS at different bias voltage

Bias [V]	P_a [kW]	P_p [kW]	V_p [V]	I_p [A]	T_s [℃]
−35	1	57.0	407	140	215
−65	1	56.6	410	138	224
−100	1	57.1	405	142	232
−130	1	55.9	411	136	245

Note— P_a and P_p: average and peak powers; V_p and I_p: peak voltage and current; T_s: average substrate temperature with no additional heat.

Thermal conductivity of Ti-Al-Si-N coatings was examined by transient thermoreflectance technique (TTR) [20]. This was a non-destructive and non-contacting optical method, which could heat the surface of the coatings and probe the surface temperature changes. Prior to thermal conductivity testing, a 100 nm thick Au film was deposited by magnetron sputtering on top of each Ti-Al-Si-N coating sample. Due to its high chemical stability, high heat reflectivity and large thermoreflectance signal, Au film was chosen as the top layer for deducing the thermal properties of the coatings. Fig. 1 shows more details of TTR measurement system. The heating laser was an ultra-compact pulsed laser, with a wavelength of 1064 nm, a pulse width of 8 ns, a single pulse energy of 50 mJ, and a frequency of 1–20 Hz. The detection laser was a continuous He-Ne laser with a wavelength of 632 nm, and a power of 1.8 mW. The heating laser was directly

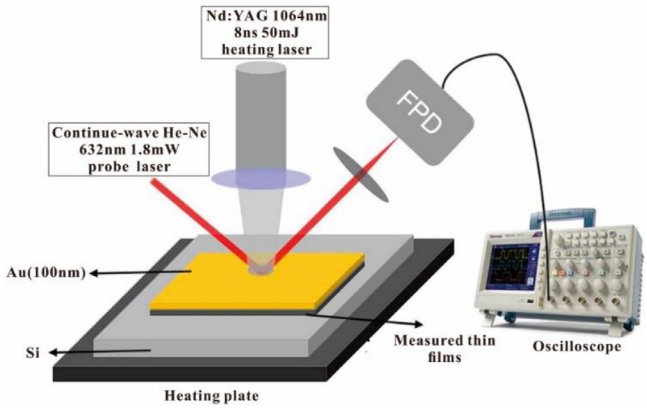

Fig. 1. Illustration of the transient thermoreflectance technique.

Table 2
Chemical composition of Ti-Al-Si-N coatings by MPPMS at different bias voltage

Bias (V)	Ti [at.%]	Al [at.%]	Si [at.%]	N [at.%]	O [at.%]
−35	17.9 ± 0.2	25.9 ± 0.3	4.8 ± 0.1	50.3 ± 0.7	1.1
−65	18.2 ± 0.5	26.1 ± 0.7	4.7 ± 0.1	50.1 ± 1.2	0.9
−100	17.9 ± 0.4	26.2 ± 0.5	4.8 ± 0.1	51.1 ± 1.8	0.7
−130	18.0 ± 0.2	25.3 ± 0.6	5.1 ± 0.1	50.5 ± 0.9	1.4

irradiated on the surface of the Au layer, causing a rise in temperature. As the heat was conducted to the film layer, the surface temperature decayed with time, and the temperature decay process was directly related to the thermal performance of the sample. Since the reflectivity of the metal was highly sensitive to the temperature, the reflectivity was substantially linear with temperature over a wide but limited temperature range, so the reflected light intensity curve could reflect the change in temperature as well. The signal of the photo detector was output to the oscilloscope, and the oscilloscope was connected to the computer to perform data fitting and analysis. The thermal characteristic parameters of the coatings could be obtained by fitting the temperature decay curve, such as thermal conductivity, contact thermal resistance, etc. The electric resistivity of Ti-Al-Si-N nanocomposite coatings was measured by four-probe method.

3. Results

3.1. Composition and microstructure

The contents of Ti-Al-Si-N coatings deposited at the bias voltages of −35 V, −65 V, −100 V and −130 V were illustrated in the Table 2. A $Ti_{0.18}Al_{0.26}Si_{0.05}N_{0.51}$ content was discovered in the coatings at the bias voltage of −35 V. As the bias voltage increased, the composition of Ti, Al, Si and N of coatings had a slight fluctuation, 17.9–18.4 at.%, 25.3–26.2 at.%, 4.6–5.1 at.%, and 50.4–51.3 at.%, respectively. The Al/(Ti + Al) composition ratio was around 0.59, that was a useful factor affecting the structure and grain size of coatings [9,21]. Chen et al. [22] found that the TiAlN films under different deposition conditions maintained a higher Al/Ti ratio than that of $Ti_{0.5}Al_{0.5}$ target, due to the different states of scattering and angular distribution for the Al and Ti particles in the magnetron sputtering process, which caused a great discrepancy of Al/Ti ratio compared with that of the bulk target.

Fig. 2 displays the XRD patterns of the Ti-Al-Si-N coatings prepared at the bias voltage from −35 V to −130 V. There were cubic TiAlN (111), (200), (220) and wurtzite AlN (002) diffraction peaks observed in the coatings besides the peak of Si substrate, however, diffraction peaks of SiN_x phases were not observed in the coatings. It was suggested that silicon may exist as an amorphous silicon nitride [23]. At the bias

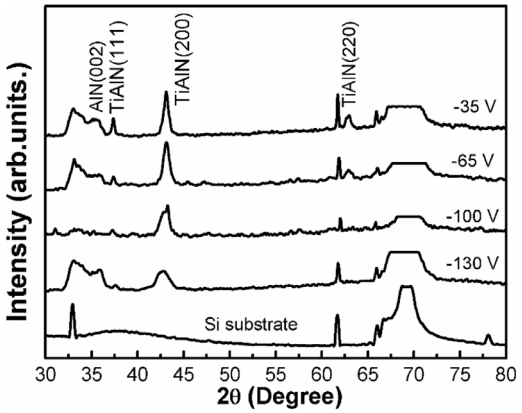

Fig. 2. The XRD patterns of Ti-Al-Si-N coatings deposited at different bias voltages.

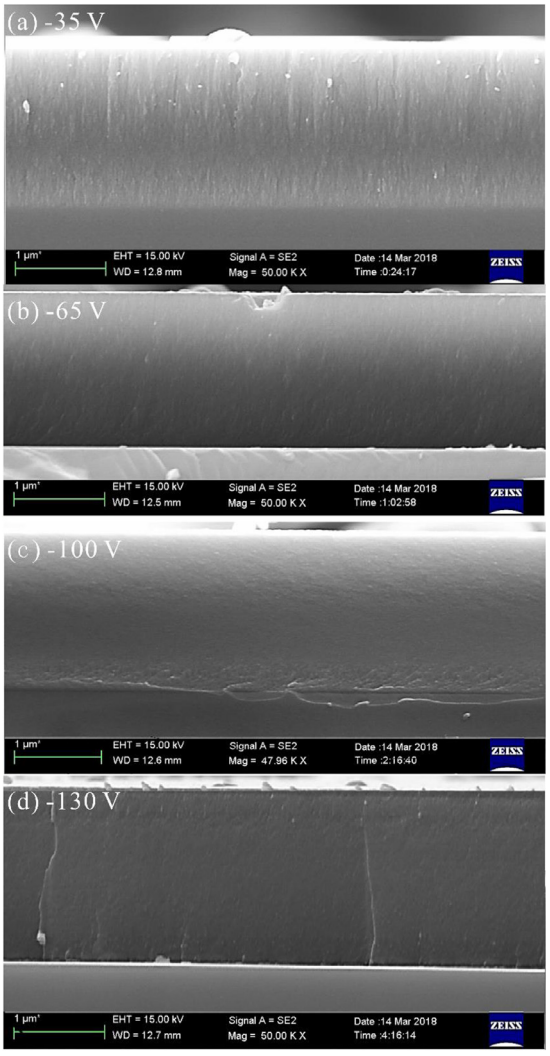

Fig. 3. The cross-sectional SEM images of Ti-Al-Si-N coatings deposited at different bias voltages.

of −35 V, the diffraction peak c-TiAlN (200) was strong and narrowed, which indicated a high crystallization of the coating. With increasing the bias voltage, the intensity of all peaks gradually decreased meanwhile the width of peaks became wider, especially the (220) peak was substantially invisible at −100 V and −130 V, the broadening of peaks was mainly caused by the decrease of grain size, due to the enhancement of bombardment energy with the bias voltage [24]. The peak intensity ratios of c-TiAlN (111) and (220) to (200) were both less than 0.25 in all the Ti-Al-Si-N coatings, the two ratios values in the standard pattern were 0.7 and 0.45, which represented the formation of a (200) preferred orientation in the Ti-Al-Si-N coatings. For transition metal nitrides, the surface free energy of (200) planes is lower than that of (111) and (220) planes [25], energetic ions bombardment induced by the bias voltage has enhanced surface diffusion in the deposition process, thereby the adatoms could accommodate in the (200) planes more easily.

As shown in the cross-sectional SEM images of Fig. 3, thickness of Ti-Al-Si-N coatings slightly increased from 1.8 μm to 1.9 μm. The thickness of coatings was an important factor that affected the thermal conductivity, which usually increased with the thickness. As can be seen from the figure, there were no voids in all coatings and the microstructure was dense. At the bias of −35 V, a very fine columnar morphology of Zone I in the ext ended structure zone model (SZM) was observed in the Ti-Al-Si-N coatings [26]. The columnar microstructure

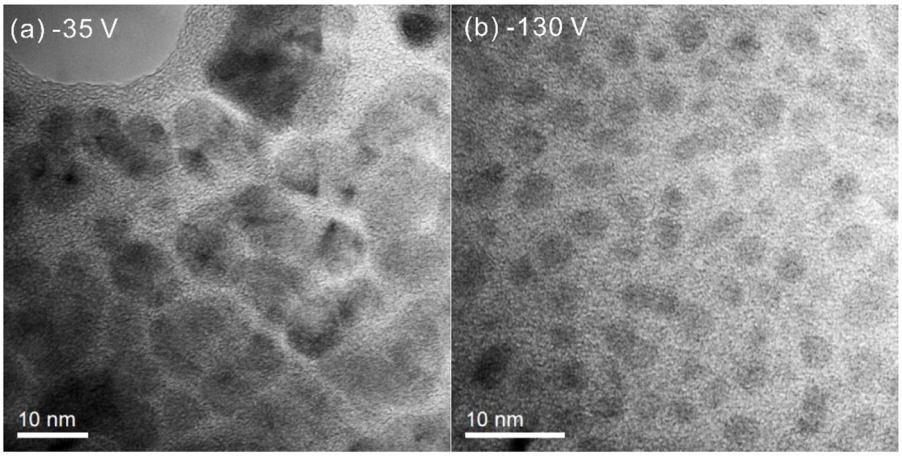

Fig. 4. The planar-view HRTEM images of Ti-Al-Si-N coatings deposited at different bias voltages.

was difficult to observe at −65 V bias compared with that at −35 V, the fractured cross section looked featureless. At the bias of −100 V and −130 V, the fractured cross sections were flat and no columnar structure was observed, which was a Zone T structure. With the increase of bias voltage, the dense columnar structure (Zone I) of Ti-Al-Si-N coatings gradually evolved into featureless and flat cross sections structure (Zone T), which has also been observed previously in Ti-Al-Si-N coatings deposited by HiPIMS [24].

Fig. 4 displays the planar-view TEM patterns of the Ti-Al-Si-N coatings deposited at the bias voltages from −35 V to −130 V. As shown in HRTEM graphics, there were no voids with a dense microstructure in the coatings, same as the results of SEM. A nanocomposite structure was found in the Ti-Al-Si-N coatings, which was consisted of amorphous phase SiN_x wrapped polycrystalline TiAlN. The TiAlN grain size was around 15–20 nm at the bias of −35 V, and decreased to about 5 nm as the bias increased to −130 V. In this paper, the ionization rate of MPPMS plasma was as high as 80%. As the bias voltage increased, the bombardment energy of ions was obviously enhanced, which improved the migration ability of particles on the surface of coatings and resulted in the refinement of grain. Grain size was an essential factor for the properties of hard coatings, such as hardness, residual stress and thermal conductivity [27,28].

3.2. Mechanical property and residual stress

Fig. 5 illustrates the hardness H, the effective elastic modulus E*, the H/E* value and the residual stress σ of the Ti-Al-Si-N nanocomposite coatings deposited at bias voltages from −35 V to −130 V. With increasing the bias voltage, the hardness increased from 31.2 GPa to 37.5 GPa, the H/E* values raised from 0.079 to 0.090. At the bias voltage of −130 V, the coating exhibited the highest hardness and the ratio H/E* of 37.5 GPa and 0.09, respectively. From Fig. 5(b), the residual stress of coatings was compressive stress and raised from −1.22 GPa to −2.15 GPa with the increase of bias voltage. The compressive stress was proportion to the hardness values of Ti-Al-Si-N coating. The increase of mechanical properties is mainly due to the increase of compressive residual stress and the reduction of grain size in Ti-Al-Si-N coatings [29]. Recently, the H/E* ratio, the residual σ and the macrostructure have been considered as indicators for determining the toughness and wear resistance of hard coatings [5,18,30]. The Ti-Al-Si-N coatings with high values of H/E* and dense macrostructure exhibited enhanced resistances to crack and wear.

3.3. Thermal conductivity

The fitting results and normalized experimental data for Ti-Al-Si-N coatings at the bias voltages from −35 V to −130 V were shown in

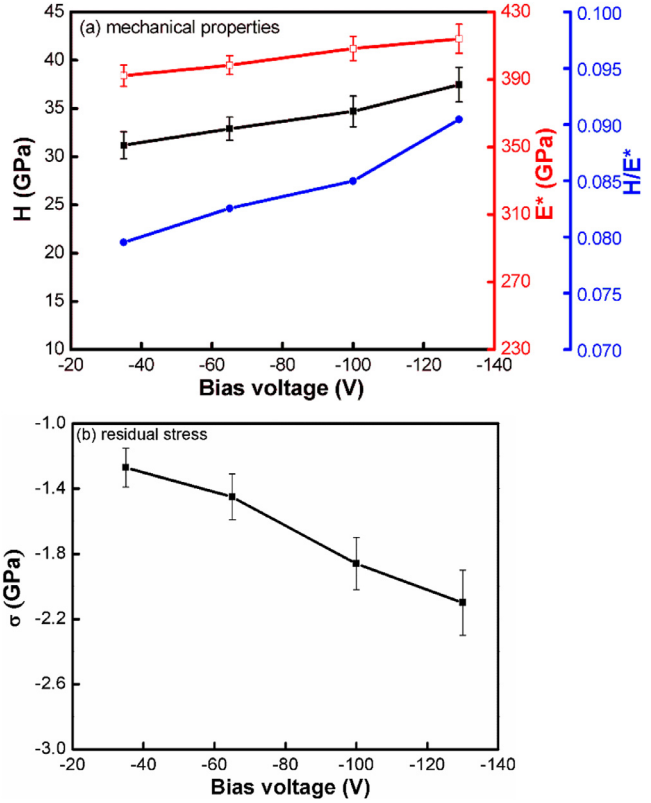

Fig. 5. The mechanical property and residual stress of Ti-Al-Si-N coatings deposited at different bias voltages.

Fig. 6. A Au/TiAlSiN/Si(100) three-layer heat conduction model was used to fit the temperature profile for obtaining the thermal conductivity of Ti-Al-Si-N coatings, which has been described in the experimental procedures. Before formal fitting, some parameters of the Au layer and the Si substrate at room temperature should be known, such as density, specific heat capacity and thermal conductivity. The averaged thermal conductivity of Au film and Si substrate was 237 W/m*K and 148 W/m*K, the bulk density and specific heat of Au film and Si substrate were 2.49×10^6 J/m^3·K and 1.659×10^6 J/m^3·K, respectively [31]. The temperature decay curve of the coatings represented the state of heat diffusion in the coatings. The deviation between experimental data and fitting results evaluated was less than 20% for all samples. From the fitting curve, the surface temperature of Ti-Al-Si-N coatings at −35 V decreased faster than that at −130 V.

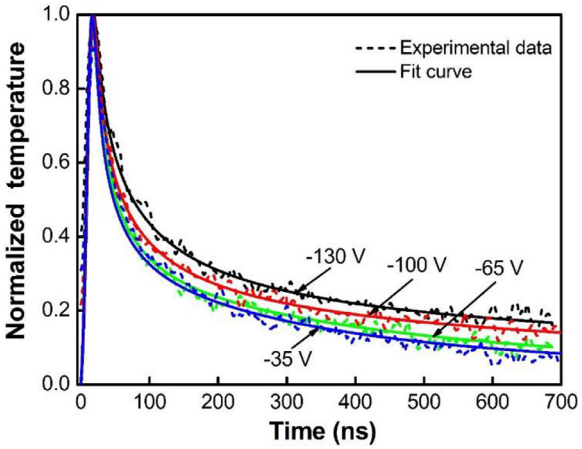

Fig. 6. The normalized measured data and fitting results of Ti-Al-Si-N coatings deposited at different bias voltages.

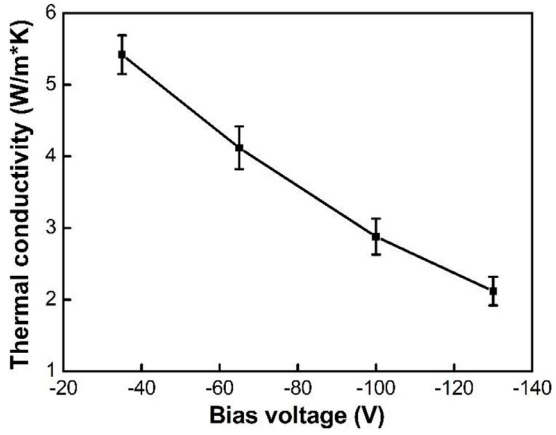

Fig. 7. The thermal conductivity of the Ti-Al-Si-N nanocomposite coatings deposited at different bias voltages.

Fig. 7 shows the thermal conductivity of Ti-Al-Si-N coatings prepared at bias voltages from −35 V to −130 V. Thermal conductivity of Ti-Al-Si-N coatings was 5.4 W/m*K at the bias of −35 V, it could be seen that the thermal conductivity decreased rapidly with the increase of bias voltage. At −130 V, Ti-Al-Si-N coatings had a lowest thermal conductivity of 2.1 W/m*K. The range of values of thermal conductivity for Ti-Al-Si-N coatings was close to that reported by Samani et al. [14]. For the cutting applications, a low thermal conductivity of nanocomposite coatings can reduce heat flow into the cutting tool, thus decreasing the temperature of cutting edge [32].

4. Discussion

From the results in Fig. 7, the thermal conductivity of Ti-Al-Si-N nanocomposite coatings decreased from 5.4 W/m*K to 2.1 W/m*K with bias voltage. For most materials, thermal conductivity was mainly consist of phonon, electronic and photon thermal conductivities, which were shown in the following formula [33],

$$k = k_{ph} + k_e + k_r, \tag{1}$$

where k_{ph}, k_e and k_r were the phonon, the electronic and the photon thermal conductivities, respectively. Photon heat transfer had a significant effect on thermal conductivity only at high temperatures, so the discussion of thermal conductivity would focus on the influence of electrons and phonons below.

The electron thermal conductivity was mainly affected by the electrical conductivity of materials at fixed temperature, as shown in

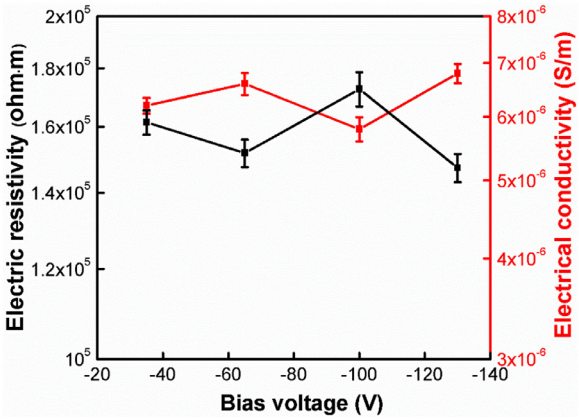

Fig. 8. The electric resistivity and conductivity of the Ti-Al-Si-N nanocomposite coatings deposited at different bias voltages.

Eq. (2). Fig. 8 shows the electric resistivity and conductivity of Ti-Al-Si-N coatings prepared at the increasing bias voltages from −35 V to −130 V. It was obvious that the electric resistivity ρ of all coatings was very large, ranging from 147 kΩ·m to 173 kΩ·m. The electric conductivity σ was calculated from $\sigma \propto 1/\rho$, which was from 5.8×10^{-6} S/m to 6.8×10^{-6} S/m. According to the law of Wiedemann–Franz, the electron thermal conductivity could be calculated by the following formula [34]:

$$k_e = LT\sigma = \frac{\pi^2}{3}\left(\frac{k_B}{e}\right)^2 \sigma T, \tag{2}$$

where σ is the electronic conductivity (S/m), T the Kelvin temperature, here is room temperature of 300 K, and L the Lorenz number of 1.48×10^{-8} W·Ω/K^2. Calculated from the Eq. (2), the electronic thermal conductivity was about 2.7×10^{-11} W/m*K, which had no contribution for the total thermal conductivity. Therefore, we can conclude that the thermal conductivity was mainly determined by the phonon thermal conductivity, not the electrons and photons.

As mentioned above, phonon heat conduction was the key factor affecting the thermal conductivity for Ti-Al-Si-N nanocomposite coatings, which can be obtained from the kinetic theory as follows. The structure of nanocomposite coatings, particularly the grain size of coatings, plays an important role in determining the phonon thermal conductivity of coatings [35],

$$k_{ph} = \frac{1}{3}\int C(\omega)\upsilon(\omega)\Lambda(\omega)d\omega \approx \frac{1}{3}C\upsilon\Lambda, \tag{3}$$

where C is the specific heat per unit volume, v the phonon velocity, and Λ the phonon mean free path. For all Ti-Al-Si-N nanocomposite coatings, due to the composition and phase structure did not change substantially, the specific heat per unit volume C and phonon velocity v of all nanocomposite coatings could be regarded as the same, so thermal conductivity k was a function of mean free path of phonon Λ.

$$\Lambda = \frac{2d}{3\varphi}, \tag{4}$$

where d is the diameter of the nanoparticles, namely the grain size, and φ is the volume fraction of nanoparticles. Because the content of the TiAlN crystal phase is very close, φ could be regarded as the same. In all the TiAlSiN nanocomposite coatings, the volume fraction of amorphous SiN_x is relatively low due to the Si content of only 5 at.%. According to Cheng and Vachon's theory of thermal conductivity for two-phase nanocomposite, the effect of amorphous SiN_x on the thermal conductivity is significantly smaller than that of the nanoparticles TiAlN [36].

Fig. 9 shows the relationship between the average grain size and thermal conductivity of Ti-Al-Si-N nanocomposite coatings at bias voltages from −35 V to −130 V. With the increase of bias voltage, the

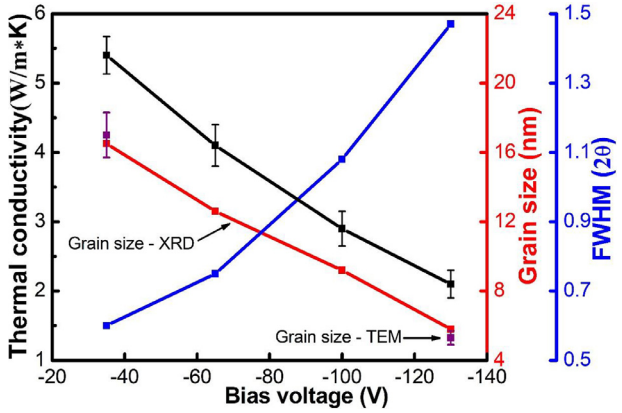

Fig. 9. The relationship between the grain size and thermal conductivity of Ti-Al-Si-N nanocomposite coatings at different bias voltages.

thermal conductivity of coatings decreased rapidly. From the XRD patterns in Fig. 2, the intensity of all the peaks gradually decreased and the width of peaks became wider with the bias voltage. Meanwhile the full width at half maximum (FWHM) of the preferential orientation TiAlN (200) increased from 0.6° to 1.5°, implying that the grain size was gradually reduced. From the Scherrer equation, the average grain size of TiAlN nanoparticles can be calculated from FWHM values of XRD peaks, which decreased from 16.5 nm to 5.8 nm as the bias voltage increased from −35 V to −130 V. The grain size of TiAlN nanoparticles from high-resolution TEM (HRTEM) images were about 15–20 nm and 5 nm at the bias voltages of −35 V and −130 V, generally consistent with that of XRD peaks. The thermal conductivity and grain size of Ti-Al-Si-N coating were positively correlated. When the grain size in the Ti-Al-Si-N nanocomposite coatings reduced, the thermal conductivity value had a decreased trend.

Jeng et al. [37] has reported the effect of nanoparticles size on the thermal conductivity of nanocomposite materials. It was obvious that the thermal conductivity gradually decreased with the decrease of grain size at the same volume fraction of nanoparticles. In order to gain an intuitive understanding into the correlation among the TiAlN nanoparticles size d (2R), volume fraction and matrix separation S, a simple model of nanocomposite had been established as shown in Fig. 10. The volume fraction of nanoparticles was the same in both coatings, but the grain size in Fig. 10(a) was twice of that in Fig. 10(b), meanwhile the matrix separation S in the former coating was also twice of that in the latter coating. Therefore, the phonons in Fig. 10(a) experienced much more scattering in unit area than that in Fig. 10(b). This mean that the interface scattering of phonons increased with the reduction in grain size, which lead to the decrease of thermal conductivity of nanocomposite coatings. In recent studies, the interface density, which mean the surface area of the nanocrystalline per unit volume in the composite shown in Fig. 10, was the major factor in affecting the thermal conductivity of nanocomposite coatings [35]. The interface density was primarily related to the volume content and the grain size of nanocrystalline.

$$\Phi = \frac{6\varphi}{d}, \tag{5}$$

In other words, with the same volume fraction of nanoparticles, the interface density is inversely proportional to the grain size. The smaller the grain size, the larger the interface density ratio, and the phonon would experience more interface scattering during heat transport process. In summary, as increasing the bias voltage, the decrease of grain size leads to an increase in the interfacial density of Ti-Al-Si-N nanocomposite coatings, resulting in the increase of phonon scattering, which is the key parameter in determining thermal conductivity of Ti-Al-Si-N nanocomposite coatings.

5. Conclusions

The Ti-Al-Si-N nanocomposite coatings were prepared by MPPMS at the bias voltages from −35 V to −130 V, the contents of coatings remained essentially unchanged, maintained as a constant of $Ti_{0.18}Al_{0.26}Si_{0.05}N_{0.51}$. With increase of the substrate bias voltage, the Ti-Al-Si-N coatings had a decrease in (200)-preferred orientation, the dense columnar structure (Zone I) of Ti-Al-Si-N coatings gradually evolved into featureless and flat cross sections structure (Zone T). With the increase of the substrate bias voltage, the hardness increased from 31.2 GPa to 37.5 GPa, the H/E* value raised from 0.079 to 0.090, meanwhile the compressive residual stress of Ti-Al-Si-N coatings raised from −1.22 GPa to −2.15 GPa. Thermal conductivity of Ti-Al-Si-N coatings was examined by transient thermoreflectance technique (TTR), which decreased from 5.4 W/m*K to 2.1 W/m*K. At the bias of −130 V, the coatings exhibited the highest hardness and the lowest thermal conductivity. As the substrate bias voltage increased, the grain sizes of Ti-Al-Si-N nanocomposite coatings decreased from 16 nm to 5 nm, the electric resistivity ρ of all coatings was very large, ranging

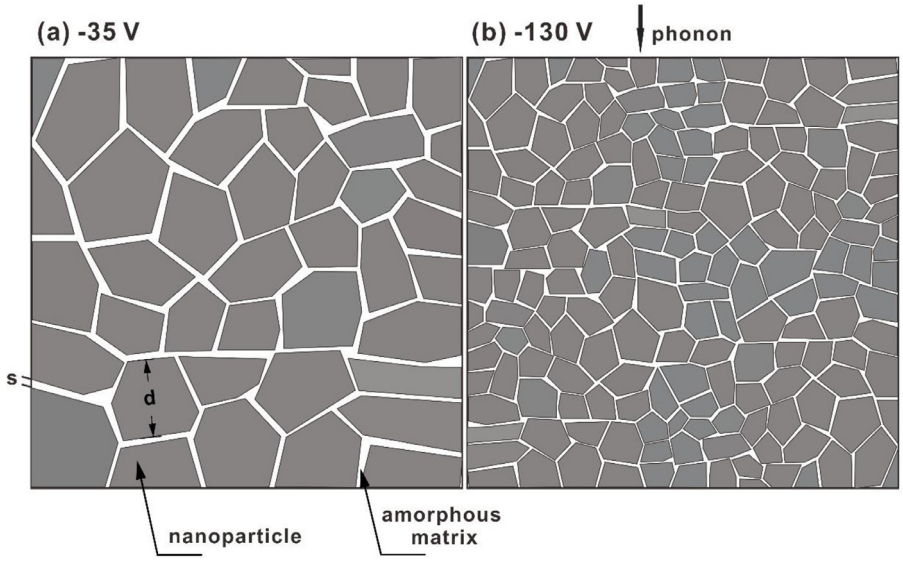

Fig. 10. A model to explain the effect of grain size on the interfacial density per unit volume in Ti-Al-Si-N nanocomposite coatings.

from 147 kΩ·m to 173 kΩ·m. The electronic thermal conductivity had no contribution for the total thermal conductivity, mainly by phonon heat conduction. The reduction of grain sizes increased the interfacial density of coatings and led phonons to experience more interface scattering in the heat transport progress. This is the key parameter in determining thermal conductivity of Ti-Al-Si-N nanocomposite coatings.

Declaration of Competing Interest

The authors declared that they have no conflicts of interest to this work.

We declare that we do not have any commercial or associative interest that represents a conflict of interest in connection with the work submitted.

Acknowledgments

The authors thank technical assistance of master students X. Y. Quan in this study. This work is supported by the National Natural Science Foundation of China under Grants no. 51575077 and 51601029.

References

[1] H. Çalişkan, C. Kurbanoğlu, P. Panjan, M. Čekada, D. Kramar, Wear behavior and cutting performance of nanostructured hard coatings on cemented carbide cutting tools in hard milling, Tribol. Int. 62 (2013) 215–222, https://doi.org/10.1016/j.triboint.2013.02.035.

[2] Y.Y. Chang, H.M. Lai, Wear behavior and cutting performance of CrAlSiN and TiAlSiN hard coatings on cemented carbide cutting tools for Ti alloys, Surf. Coat. Technol. 259 (2014) 152–158, https://doi.org/10.1016/j.surfcoat.2014.02.015.

[3] R. Franz, C. Mitterer, Vanadium containing self-adaptive low-friction hard coatings for high-temperature applications: a review, Surf. Coat. Technol. 228 (2013) 1–13, https://doi.org/10.1016/j.surfcoat.2013.04.034.

[4] H. Çalişkan, C. Kurbanoğlu, P. Panjan, D. Kramar, Investigation of the performance of carbide cutting tools with hard coatings in hard milling based on the response surface methodology, Int. J. Adv. Manuf. Technol. 66 (2013) 883–893, https://doi.org/10.1007/s00170-012-4374-y.

[5] J. Musil, Hard nanocomposite coatings: thermal stability, oxidation resistance and toughness, Surf. Coat. Technol. 207 (2012) 50–65, https://doi.org/10.1016/j.surfcoat.2012.05.073.

[6] S. Zhang, D. Sun, Y. Fu, H. Du, Recent advances of superhard nanocomposite coatings: a review, Surf. Coat. Technol. 167 (2003) 113–119, https://doi.org/10.1016/S0257-8972(02)00903-9.

[7] S. Veprek, M.G.J. Veprek-Heijman, P. Karvankova, J. Prochazka, Different approaches to superhard coatings and nanocomposites, Thin Solid Films 476 (2005) 1–29, https://doi.org/10.1016/j.tsf.2004.10.053.

[8] S. Veprek, H. Männling, M. Jilek, P. Holubar, Avoiding the high-temperature decomposition and softening of $(Al_{1-x}Ti_x)$ N coatings by the formation of stable superhard nc-$(Al_{1-x}Ti_x)$ N/a-Si_3N_4 nanocomposite, Mater. Sci. Eng. A. 366 (2004) 202–205, https://doi.org/10.1016/j.msea.2003.08.052.

[9] Y. Chang, S. Yang, High temperature oxidation behavior of multicomponent TiAlSiNcoatings, Thin Solid Films 518 (2010) S34–S37, https://doi.org/10.1016/j.tsf.2010.03.020.

[10] X. Sui, G. Li, X. Qin, H. Yu, X. Zhou, K. Wang, Q. Wang, Relationship of microstructure, mechanical properties and titanium cutting performance of TiAlN/TiAlSiN composite coated tool, Ceram. Int. 42 (2016) 7524–7532, https://doi.org/10.1016/j.ceramint.2016.01.159.

[11] K. Bouzakis, E. Bouzakis, S. Kombogiannis, R. Paraskevopoulou, G. Skordaris, Effect of silicon content on PVD fi lm mechanical properties and cutting performance of coated cemented carbide inserts, Surf. Coat. Technol. 237 (2013) 379–389, https://doi.org/10.1016/j.surfcoat.2013.06.044.

[12] K. Bouzakis, G. Skordaris, S. Gerardis, G. Katirtzoglou, S. Makrimallakis, M. Pappa, Ambient and elevated temperature properties of TiN, TiAlN and TiSiN PVD films and their impact on the cutting performance of coated carbide tools, Surf. Coat. Technol. 204 (2009) 1061–1065, https://doi.org/10.1016/j.surfcoat.2009.07.001.

[13] G.S. Fox-rabinovich, K. Yamamoto, M.H. Aguirre, D.G. Cahill, S.C. Veldhuis, A. Biksa, Multi-functional nano-multilayered AlTiN/Cu PVD coating for machining of Inconel 718 superalloy, Surf. Coat. Technol. 204 (2010) 2465–2471, https://doi.org/10.1016/j.surfcoat.2010.01.024.

[14] M.K. Samani, X.Z. Ding, S. Amini, N. Khosravian, J.Y. Cheong, G. Chen, B.K. Tay, Thermal conductivity of titanium aluminum silicon nitride coatings deposited by lateral rotating cathode arc, Thin Solid Films 537 (2013) 108–112, https://doi.org/10.1016/j.tsf.2013.04.029.

[15] M.K. Samani, X.Z. Ding, N. Khosravian, B. Amin-ahmadi, Y. Yi, G. Chen, E.C. Neyts, A. Bogaerts, B.K. Tay, Thermal conductivity of titanium nitride / titanium aluminum nitride multilayer coatings deposited by lateral rotating cathode arc, Thin Solid Films 578 (2015) 133–138, https://doi.org/10.1016/j.tsf.2015.02.032.

[16] J. Lin, W.D. Sproul, J.J. Moore, Z. Wu, S. Lee, R. Chistyakov, B. Abraham, Recent advances in modulated pulsed power magnetron sputtering for surface engineering, JOM 63 (2011) 48–58, https://doi.org/10.1007/s11837-011-0092-4.

[17] Z.L. Wu, Y.G. Li, B. Wu, M.K. Lei, Effect of microstructure on mechanical and tribological properties of TiAlSiN nanocomposite coatings deposited by modulated pulsed power magnetron sputtering, Thin Solid Films 597 (2015) 197–205, https://doi.org/10.1016/j.tsf.2015.11.047.

[18] H. Chen, B.C. Zheng, Y.G. Li, Z.L. Wu, M.K. Lei, Flexible hard TiAlSiN nanocomposite coatings deposited by modulated pulsed power magnetron sputtering with controllable peak power, Thin Solid Films 669 (2019) 377–386, https://doi.org/10.1016/j.tsf.2018.10.031.

[19] J. Musil, M. Šašek, P. Zeman, R. Čerstvý, D. Heřman, J.G. Han, V. Šatava, Properties of magnetron sputtered Al-Si-N thin films with a low and high Si content, Surf. Coat. Technol. 202 (2008) 3485–3493, https://doi.org/10.1016/j.surfcoat.2007.12.024.

[20] Q. Li, J. Wei, H. Sun, K. Zhang, Z. Huang, L. Zhang, Temperature dependent thermal conductivity and transition mechanism in amorphous and crystalline Sb_2Te_3 thin films, Sci. Rep. 7 (2017) 13747, https://doi.org/10.1038/s41598-017-14068-7.

[21] L. Chen, J. Paulitsch, Y. Du, P.H. Mayrhofer, Thermal stability and oxidation resistance of Ti-Al-N coatings, Surf. Coat. Technol. 206 (2012) 2954–2960, https://doi.org/10.1016/j.surfcoat.2011.12.028.

[22] L. Chen, M. Moser, Y. Du, P.H. Mayrhofer, Compositional and structural evolution of sputtered Ti-Al-n, Thin Solid Films 517 (2009) 6635–6641, https://doi.org/10.1016/j.tsf.2009.04.056.

[23] H. Fager, J.M. Andersson, J. Lu, M.P.J. Jöesaar, M. Odén, L. Hultman, Growth of hard amorphous TiAlSiN thin films by cathodic arc evaporation, Surf. Coat. Technol. 235 (2013) 376–382, https://doi.org/10.1016/j.surfcoat.2013.07.014.

[24] Q. Ma, L. Li, Y. Xu, J. Gu, L. Wang, Y. Xu, Effect of bias voltage on TiAlSiN nanocomposite coatings deposited by HiPIMS, Appl. Surf. Sci. 392 (2017) 826–833, https://doi.org/10.1016/j.apsusc.2016.09.028.

[25] Q. Luo, S. Yang, K.E. Cooke, Hybrid HiPIMS and DC magnetron sputtering deposition of TiN coatings: deposition rate, structure and tribological properties, Surf. Coat. Technol. 236 (2013) 13–21, https://doi.org/10.1016/j.surfcoat.2013.07.003.

[26] J.A. Thornton, High rate thick film growth, Annu. Rev. Mater. Sci. 7 (1977) 239–260, https://doi.org/10.1146/annurev.ms.07.080177.001323.

[27] C. Mitterer, P.H. Mayrhofer, J. Musil, Thermal stability of PVD hard coatings, Vacuum 71 (2003) 279–284, https://doi.org/10.1016/S0042-207X(02)00751-0.

[28] Z. Wang, J.E. Alaniz, W. Jang, J.E. Garay, C. Dames, Thermal conductivity of nanocrystalline silicon: importance of grain size and frequency-dependent mean free paths, Nano Lett 11 (2011) 2206–2213, https://doi.org/10.1021/nl1045395.

[29] F. Cao, P. Munroe, Z. Zhou, Z. Xie, Influence of substrate bias on microstructural evolution and mechanical properties of TiAlSiN thin films deposited by pulsed-DC magnetron sputtering, Thin Solid Films 639 (2017) 137–144, https://doi.org/10.1016/j.tsf.2017.08.036.

[30] Y.X. Ou, H. Chen, Z.Y. Li, J. Lin, W. Pan, M.K. Lei, Microstructure and tribological behavior of TiAlSiN coatings deposited by deep oscillation magnetron sputtering, j, Am. Ceram. Soc. 101 (2018) 5166–5176, https://doi.org/10.1111/jace.15769.

[31] S. Bai, Z. Tang, Z. Huang, J. Yu, Thermal characterization of Si_3N_4 thin films using transient thermoreflectance technique, IEEE Trans. Ind. Electron. 56 (2009) 3238–3243, https://doi.org/10.1109/TIE.2009.2022078.

[32] S. Veprek, M.J.G. Veprek-Heijman, Industrial applications of superhard nanocomposite coatings, Surf. Coat. Technol. 202 (2008) 5063–5073, https://doi.org/10.1016/j.surfcoat.2008.05.038.

[33] C.J. Glassbrenner, G.A. Slack, Thermal conductivity of silicon and germanium from 3°K to the melting point, Phys. Rev. 134 (1964) A1058–A1069, https://doi.org/10.1103/PhysRev.134.A1058.

[34] T.M. Tritt, Experimental techniques for thin film thermal conductivity characterization, Chap. 2.2, in: T.M. Tritt (Ed.), Thermal Conductivity: Theory, Properties, and Applications, Springer US, New York, 2004, , https://doi.org/10.1007/b136496.

[35] A. Minnich, G. Chen, Modified effective medium formulation for the thermal conductivity of nanocomposites, Appl. Phys. Lett. 91 (2007) 4–7, https://doi.org/10.1063/1.2771040.

[36] S.C. Cheng, R.I. Vachon, The prediction of the thermal conductivity of two and three phase solid heterogeneous mixtures, Int. J. Heat Mass Transf. 12 (1969) 249–264, https://doi.org/10.1016/0017-9310(69)90009-X.

[37] M.S. Jeng, R. Yang, D. Song, G. Chen, Modeling the thermal conductivity and phonon transport in nanoparticle composites using Monte Carlo simulation, J. Heat Transfer. 130 (2008) 042410, , https://doi.org/10.1115/1.2818765.